optica

Adaptive-optics-based simultaneous pre- and post-turbulence compensation of multiple orbital-angular-momentum beams in a bidirectional free-space optical link

Yongxiong Ren,[1,*] Guodong Xie,[1] Hao Huang,[1] Nisar Ahmed,[1] Yan Yan,[1] Long Li,[1] Changjing Bao,[1] Martin P. J. Lavery,[1,2] Moshe Tur,[3] Mark A. Neifeld,[4] Robert W. Boyd,[2,5] Jeffrey H. Shapiro,[6] and Alan E. Willner[1,7]

[1]Department of Electrical Engineering, University of Southern California, Los Angeles, California 90089, USA

[2]School of Physics and Astronomy, University of Glasgow, Glasgow, G12 8QQ, UK

[3]School of Electrical Engineering, Tel Aviv University, Ramat Aviv 69978, Israel

[4]Department of Electrical and Computer Engineering, University of Arizona, Tucson, Arizona 85721, USA

[5]Department of Physics and Astronomy, The Institute of Optics, University of Rochester, Rochester, New York 14627, USA

[6]Research Laboratory of Electronics, Massachusetts Institute of Technology, Cambridge, Massachusetts 02139, USA

[7]e-mail: willner@usc.edu

*Corresponding author: yongxior@usc.edu

As a recently explored property of light, orbital angular momentum (OAM) has potential in enabling multiplexing of multiple data-carrying beams, to increase the transmission capacity and spectral efficiency of a communication system. For the use of OAM multiplexing in free-space optical (FSO) communications, atmospheric turbulence presents a critical challenge. In this paper, we experimentally demonstrate simultaneous pre- and post-turbulence compensation of multiple OAM beams, in a bidirectional free-space optical communications link, using a single adaptive optics (AO) system. Each beam carries a 100 Gbit/s signal, and propagates through an emulated atmospheric turbulence. A specifically designed AO system, which utilizes a Gaussian beam for wavefront sensing and correction, is built at one end of the bidirectional link. We show that this AO system can be used to not only post-compensate the received OAM beams, but also pre-compensate the outgoing OAM beams emitted from the same link end. Experimental results show that this compensation technique helps reduce the crosstalk onto adjacent modes by more than 12 dB, achieving bit error rates below the forward error correction limit of 1×10^{-3}, for both directions of the link. The results of work might be helpful to future implementation of OAM multiplexing, in a high-capacity FSO bidirectional link affected by atmospheric turbulence.   © 2014 Optical Society of America

1. INTRODUCTION

It was discovered in 1992 that a light beam, with helical transverse phase of the form $\exp(i\ell\emptyset)$, carries an orbital angular momentum (OAM) corresponding to $\ell\hbar$ per photon, where $\emptyset$ is the azimuthal angle, ℓ is the OAM topological charge (ℓ is an unbounded integer), and $\hbar$ is the reduced Planck's constant [1]. Since then, as a fundamental physical quantity in classical and quantum electrodynamics, OAM of light has initiated increased interest in many areas, including optical tweezers, atom manipulation, microscopy, and photon entanglement [2–4]. Recently, OAM has drawn the attention of the optical communications community, for its potential to efficiently multiplex many independent data streams [5–9], due to the fact that beams carrying OAM can form an orthogonal modal basis (i.e., OAM beams with different ℓ are orthogonal to one another) [5].

Previous reports have shown terabit/s free-space data transmissions, using OAM multiplexing, in the absence of atmospheric turbulence effects [6]. However, for a practical OAM multiplexed free-space optical (FSO) communications link, atmospheric turbulence presents a critical challenge [10–15]. As the orthogonality of multiple co-propagating OAM beams depends on their distinct helical phase-fronts, atmospheric turbulence that distorts these phase-fronts will cause power spreading of each transmitted OAM beam, into neighboring modes. This may result in severe inter-modal crosstalk between different OAM data channels [13–15]. Optical compensation of turbulence-induced phase front distortions may well reduce this inter-modal crosstalk. Recently, an adaptive optics (AO) system, that might be suitable for turbulence compensation of OAM beams, has been experimentally demonstrated in an unidirectional link [16,17], overcoming technical challenges resulting from the phase singularity of OAM beams [18,19].

Optical propagation through atmospheric turbulence is generally point reciprocal [20–23], i.e., the two spatial impulse responses (Green's functions) that characterize the optical propagation, in opposite directions between the transmitting and the receiving aperture planes, are equivalent. A recent experimental work on a bidirectional FSO link, with tilt/tip tracking, has led to the identification of scintillation reciprocity [22], as well as the reciprocity proof for the fundamental Gaussian mode [23]. However, there has been little reported in a bidirectional link employing spatial-mode multiplexing, with or without high-order AO compensation.

Importantly, the reciprocity of atmosphere turbulence suggests that the beams, propagating in opposite directions through the same atmosphere medium, may experience similar turbulence distortions. For an OAM multiplexed bidirectional FSO link, this might imply that the AO system, that helps compensate the distorted data-carrying OAM beams at the receiver in one direction, can potentially be used to help correct the OAM beams being transmitted in the reverse direction.

In this paper, the bidirectional turbulence compensation of multiple data-carrying OAM modes, in an FSO link through atmospheric turbulence, is investigated based on the reciprocity of turbulent atmosphere. We experimentally demonstrate that a single AO system, placed at one end of the bidirectional link, can be employed to simultaneously pre- and post-compensate multiple counter-propagating OAM beams, through emulated atmospheric turbulence [24]. Specifically, one direction of the link experiences pre-compensation [25,26], and the other direction benefits from post-compensation. Our experimental results show that for the two compensated link directions, the crosstalk onto adjacent modes can be reduced by more than 12 dB, achieving bit-error-rates (BERs) below the forward error correction (FEC) limit of 1×10^{-3}. Furthermore, we show through theoretical analysis that the turbulence-distorted OAM beams, at both ends of the bidirectional link, have identical crosstalk behavior.

2. THEORETICAL BACKGROUND AND CONCEPT

The reciprocity of atmospheric turbulence has been demonstrated in the previous theoretical analysis, and verified with experimental data, suggesting that the intensity and phase fluctuations of the received signals for Gaussian beams, at the opposite ends of a bidirectional FSO link, can be identical [22,23]. Using an approach similar to that in the previous proof of scintillation reciprocity, we analyze the crosstalk between turbulence-distorted OAM beams, in a bidirectional FSO link.

Figure 1 shows the propagation geometry. At the transmitter 1 (TX-1) side, data-carrying multiplexed OAM beams pass through a circular transmitter aperture $\mathcal{A}_1$ in the $Z = 0$ plane, and propagate over an L-m-long turbulent path. The beams arriving at $Z = L$ are first collected through a circular receiver aperture $\mathcal{A}_2$ at receiver 1 (RX-1), then pass through the AO compensation system and the OAM detection module. A similar progression applies to the opposite propagation path, namely TX-2/RX-2 link. The AO wavefront corrector, at $Z = L$, applies the same phase compensation to TX-2's outgoing OAM beams as it does to the received beams from TX-1. We assume that the OAM transmitter and receiver at each end share common-aperture optics, which means that the exit pupil for each end's transmitter is also the entrance pupil for its receiver. For simplicity, it is also assumed that both apertures $\mathcal{A}_1$ and $\mathcal{A}_2$ have the same diameter, so that a common transmitted OAM mode set can be used for each link direction. However, the analysis below can be easily extended to arbitrary distinct choices for aperture pupils [23].

Let $\{\varepsilon_\ell(\mathbf{r}_1): \ell = m_1, m_2, \ldots m_n; m_i \in \mathbb{Z}\}$ be the transmitted OAM modes group at TX-1, where n is the number of multiplexed OAM modes. Here, $\varepsilon_\ell(\mathbf{r}_1)$ carries OAM charge
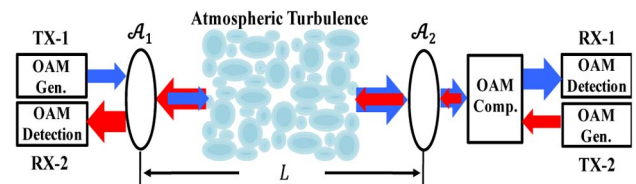

Fig. 1. Propagation geometry of a bidirectional OAM multiplexed optical communication link through atmospheric turbulence; Comp., compensation; Gen., generation; RX, receiver; TX, transmitter.

ℓ, and contains the azimuthal phase structure $\exp(i\ell\angle\mathbf{r}_1)$, with $\angle$ as the angle operator. $\varepsilon_\ell(\mathbf{r}_1)$ satisfies the normalization condition

$$\int_{\mathcal{A}_1} d\mathbf{r}_1 |\varepsilon_\ell(\mathbf{r}_1)|^2 = 1. \tag{1}$$

Also, OAM modes with different ℓ are orthogonal

$$\int_{\mathcal{A}_1} d\mathbf{r}_1 \varepsilon_{\ell'}^*(\mathbf{r}_1)\varepsilon_\ell(\mathbf{r}_1) = 0, \quad \text{for } \ell \neq \ell'. \tag{2}$$

Suppose that we transmit $\sqrt{P_T}\varepsilon_\ell(\mathbf{r}_1)$ through $\mathcal{A}_1$ at TX-1, with P_T being the power carried by OAM mode $\varepsilon_\ell(\mathbf{r}_1)$. After passing through the atmospheric turbulence, the field of the distorted OAM beam at the receiver aperture $\mathcal{A}_2$ can be expressed as

$$\int_{\mathcal{A}_1} d\mathbf{r}_1 \varepsilon_\ell(\mathbf{r}_1) h(\mathbf{r}_1, \mathbf{r}_2, t), \tag{3}$$

according to the extended Huygens–Fresnel principle [27]. Here, $h(\mathbf{r}_1, \mathbf{r}_2, t)$ is the atmosphere's spatial impulse response (Green's function) at time t. For a line-of-sight propagation delay $2L/c$ that is much shorter than an atmospheric coherence time (c is the speed of light), we can neglect and suppress the Green function's time dependence, since bidirectional transmission at time t will encounter the same atmospheric Green's function, $h(\mathbf{r}_1, \mathbf{r}_2)$ [28,29]. If AO compensation is employed, the field after compensation can be written as

$$\int_{\mathcal{A}_1} d\mathbf{r}_1 \varepsilon_\ell(\mathbf{r}_1) h(\mathbf{r}_1, \mathbf{r}_2) e^{i\varphi(\mathbf{r}_2)}, \tag{4}$$

where $\varphi(\mathbf{r}_2)$ is the phase correction term, that has been applied in the AO system, at the TX-1 side. The resulting field after AO compensation is then sent for OAM detection. Ideally, the power leaked to OAM mode ℓ' is determined by the $\varepsilon_{\ell'}(\mathbf{r}_2)$ component of the field in $\mathcal{A}_2$ [23]

$$^1P_{\ell \to \ell'} = P_T \left| \int_{\mathcal{A}_2} d\mathbf{r}_2 \varepsilon_{\ell'}^*(\mathbf{r}_2) \int_{\mathcal{A}_1} d\mathbf{r}_1 \varepsilon_\ell(\mathbf{r}_1) h(\mathbf{r}_1, \mathbf{r}_2) e^{i\varphi(\mathbf{r}_2)} \right|^2. \tag{5}$$

The power-transfer behavior of the OAM beams, for the TX-2/RX-2 link, can be derived with the use of a similar approach. Here, we need to use $\{\varepsilon_{\ell'}^*(\mathbf{r}_2) : \ell' = m_1, m_2, \ldots m_n; m_i \in \mathbb{Z}\}$ for the transmitted OAM mode group at TX-2, where $\varepsilon_{\ell'}^*(\mathbf{r}_2)$ carries OAM charge ℓ'. If the same phase correction is used for the transmission of $\sqrt{P_T}\varepsilon_{\ell'}^*(\mathbf{r}_2)$ from TX-2, we obtain

$$^2P_{\ell' \to \ell} = P_T \left| \int_{\mathcal{A}_1} d\mathbf{r}_1 \varepsilon_\ell(\mathbf{r}_1) \int_{\mathcal{A}_2} d\mathbf{r}_2 \varepsilon_{\ell'}^*(\mathbf{r}_2) h(\mathbf{r}_2, \mathbf{r}_1) e^{i\varphi(\mathbf{r}_2)} \right|^2, \tag{6}$$

for the power extracted in the $\varepsilon_\ell^*(\mathbf{r}_1)$ mode within $\mathcal{A}_1$. We can see that given $h(\mathbf{r}_1, \mathbf{r}_2) = h(\mathbf{r}_2, \mathbf{r}_1)$ [20], $^1P_{\ell \to \ell'}$ for the post-compensated TX-1/RX-1 link is identical to $^2P_{\ell' \to \ell}$ for the pre-compensated TX-2/RX-2 link

$$^1P_{\ell \to \ell'} = {}^2P_{\ell' \to \ell}. \tag{7}$$

This equivalence prevails for all $\varphi(\mathbf{r}_2)$, including $\varphi(\mathbf{r}_2) = 0$, that corresponds to the case without AO compensation. The validity of Eq. (7) requires that the OAM generation and detection modules, for the TX-1/RX-1 link, are symmetrically built with those of the TX-2/RX-2 link. Any asymmetry, in the OAM generation or detection modules of the two link directions, is expected to result in performance differences between them. Similarly to the previous analysis for a non-OAM bidirectional FSO link, the power transfer reciprocity of OAM beams implied from Eq. (7) applies for any atmospheric state, regardless of the strength of the turbulence, its distribution along the transmission path, and the size of transmitter (and receiver) apertures. However, one critical condition for this reciprocity property is the frozen-turbulence assumption, which requires that the turbulence state remains the same, over the entire propagation delay period. In general, this condition is not problematic if the propagation delay of this link is sufficiently short, compared with the typical turbulence coherence time.

Equation (7) guarantees that the received OAM beams, emitted from both directions in a bidirectional link, have identical crosstalk behavior after propagating through the same atmospheric turbulence. It is valid for cases with and without AO phase compensation. It also implies that a single AO system, that post-compensates beams emitted from one direction, can simultaneously pre-compensate multiple OAM beams propagating in the opposite direction.

The concept of simultaneous pre- and post-compensation of multiplexed OAM beams, using a single AO system, is illustrated in Fig. 2. Multiple data-carrying OAM beams are generated (and multiplexed) at TX-1 and TX-2, respectively. These two groups of OAM beams coaxially propagate through atmospheric turbulence, in opposite directions. An AO compensation system, placed at one end of the link (TX-2 side), is used to compensate the received turbulence-distorted OAM beams from TX-1 (post-compensation). The outgoing OAM
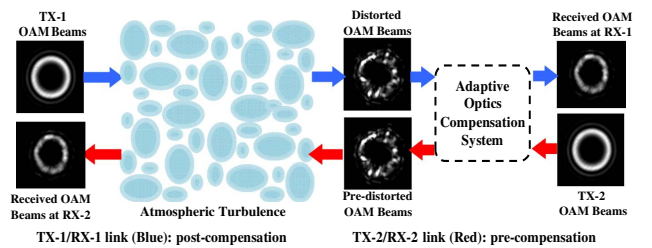

Fig. 2. Concept diagram. One group of multiplexed data-carrying OAM beams from TX-1 is first distorted by atmospheric turbulence, and then compensated by the AO system (post-compensation). Another group of OAM beams from TX-2 first experiences pre-compensation by the AO system, and then propagates through the same turbulence (pre-compensation). RX, receiver; TX, transmitter.

beams from TX-2 are first spatially phase modulated, by the wavefront corrector element inside the AO system (i.e., pre-compensation [25,26]), and then propagate through the same turbulent atmosphere. The two received OAM beam groups, at RX-1 and RX-2, are subsequently demultiplexed and detected.

3. EXPERIMENTAL SETUP

The experimental setup is presented in Fig. 3. A narrow line-width laser at 1550 nm is sent to a Mach–Zehnder modulator, to produce a 100-Gbit/s quadrature phase-shift keying (QPSK) signal at the TX-1 side. This signal is split into three copies, each of which is decorrelated using single-mode fibers (SMFs) with different lengths. The three polarized signal copies are sent to three collimators, each converting the SMF output to a collimated Gaussian beam, with a beam diameter of 3 mm. Two of the three beams (branch ① and ②) are launched onto two equally divided regions of a reflective spatial light modulator (SLM-1), respectively. Specifically, one beam (branch ①) is incident onto one half of SLM-1, loaded with a specific blazed-fork hologram, to create one OAM beam ($\ell = 3$ or $\ell = 5$). Another beam (branch ②) is converted into a superposition of two equally-weighted OAM beams (with $\ell = 3, 7$, or $\ell = 1, 9$), by loading the other half of SLM-1 with an appropriately designed phase hologram [30]. Branch ② is only turned on when investigating the impact of OAM crosstalk, on the BER performance of the multiplexed OAM channels. The Gaussian beam in branch ③ is polarization rotated using a half-wave plate (HWP-1), and then expanded using a 4-f lens system, to become as wide as the widest OAM beam (i.e., $\ell = 9$ in this experiment) along the propagation path. This branch is then polarization multiplexed with branches ① and ②, via a polarization beam splitter (PBS), and propagates coaxially with the OAM beams.

At the TX-2 side, a similar OAM-multiplexing module is built, where three 100-Gbit/s data-carrying OAM beams at 1550 nm are generated by SLM-2, and are multiplexed using beam splitters. The resulting multiplexed beams, transmitted from TX-1 and TX-2, coaxially counter-propagate through the turbulence emulator and the AO system. The effects of

turbulence are emulated by a rotatable thin phase screen plate, with a pseudo-random phase distribution obeying Kolmogorov spectrum statistics, and characterized by its effective Fried coherence length r_0 [27–29]. In our experiment, r_0 is set to be 1 mm, which could represent weak-to-moderate turbulence over a 1 km link distance [14] (see Supplement 1).

The closed-loop AO system is specifically designed and placed at TX-2 side, to compensate the beams emitted from TX-1. In the AO system, the distorted received Gaussian beam is separated from the incoming OAM beams, using a PBS to serve as the probe for wavefront-distortion estimation, from which the required correction patterns are retrieved (Supplement 1 has more details) [16]. A feedback controller is used for communication between wavefront sensor and SLM-3, to provide the correction pattern. For each turbulence realization, the correction pattern (obtained from the Gaussian beam) is used to compensate the distorted OAM beams emitted from TX-1. The corrected OAM beams are then sent to SLM-4, which is loaded with an inverse spiral phase hologram of that particular OAM channel, chosen to be detected for BER measurement. This OAM beam is thus converted by SLM-4 to a Gaussian-like beam [4], which is coupled into a SMF, and sent for coherent detection (and off-line digital signal processing) at RX-1. On the way from the AO compensation system to SLM-4, an infrared camera, fed by a flip mirror, is used to capture far-field intensity profiles of the compensated beams.

Unlike the light path of the multiplexed beams from TX-1, the outgoing beams from TX-2 are sent to the AO system, and then propagate through the turbulence emulator. Consequently, the outgoing beams are first pre-distorted by the correction patterns on SLM-3, inside the AO system, before experiencing the turbulence distortions (i.e., pre-compensation). After passing through the turbulence emulator, the beams are sent to SLM-5 for demultiplexing and data recovery at RX-2.

4. EXPERIMENTAL RESULTS

Figure 4 shows far-field intensity profiles and interferograms of the OAM beams ($\ell = 3$ and 5), for a random turbulence realization, with and without pre- and post-compensation.
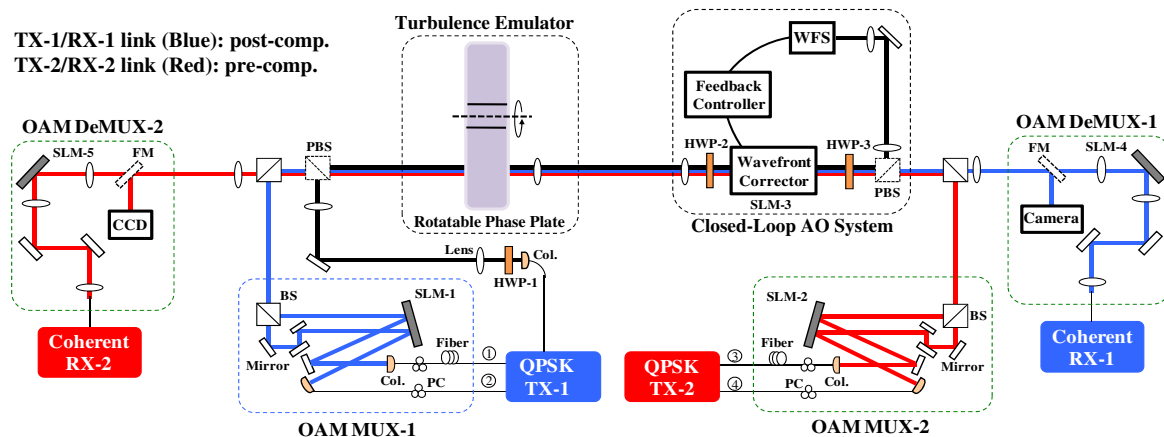

Fig. 3. Experimental setup; AO, adaptive optics; BS, beam-splitter; Col, Collimator; DeMUX, Demultiplexer; FM, flip mirror; HWP. half wave plate; MUX, multiplexer; OC, optical coupler; PBS, polarizing beam splitter; PC, polarization controller; QPSK, quadrature phase-shift keying; RX, receiver; SLM, spatial light modulator; TX, Transmitter; WFS, Shack–Hartmann wavefront sensor.

The interferograms of the OAM beams $\ell = 3$ and 5, without experiencing turbulence distortions, are also shown. In Fig. 4, branches ① and ③ generate OAM beams with the same ℓ (either $\ell = 3$ or $\ell = 5$), and branches ② and ④ are turned off. The interferograms are obtained from interfering OAM beams with an expanded Gaussian beam. From the far-field images, we see that the distorted OAM beams [Figs. 4(a1), (a2), (b1), and (b2)] are efficiently compensated [Figs. 4 (a5), (a6), (b5), and (b6)], for both the TX-1/RX-1 and TX-2/RX-2 links. The interference patterns shown in Figs. 4 (a7), (a8), (b7), and (b8), compared with those shown in Figs. 4 (a3), (a4), (b3), (b4), (c1) and (c2), verify that the OAM wavefront errors, especially the dominant terms, i.e., turbulence-induced tip/tilt, have been corrected. We note that the post-compensation for the TX-1/RX-1 link exhibits slightly better performance than the pre-compensation for the TX-2/RX-2 link. This observation is also corroborated by the crosstalk and BER measurements reported below.

Figure 5(a) presents the received power fluctuations of OAM channel $\ell = 5$ for each link, when only OAM beam $\ell = 5$ is transmitted, under 10 different turbulence realizations, with and without compensation. In Fig. 5(a), SLM-4 is loaded with a spiral phase hologram of $\ell = -5$, to convert the OAM beam $\ell = 5$ into a Gaussian-like beam, that is then coupled into an SMF for power measurement. We observe that the received powers for both links fluctuate without compensation, and remain fairly stable after pre- or post-compensation. Figure 5(b) depicts the crosstalk from the OAM $\ell = 5$ channel to neighboring channels, for each link direction, under a random turbulence realization, with and without compensation. We see that without compensation, the incident power of the OAM channel $\ell = 5$, for both link directions, is coupled to other neighboring OAM channels,
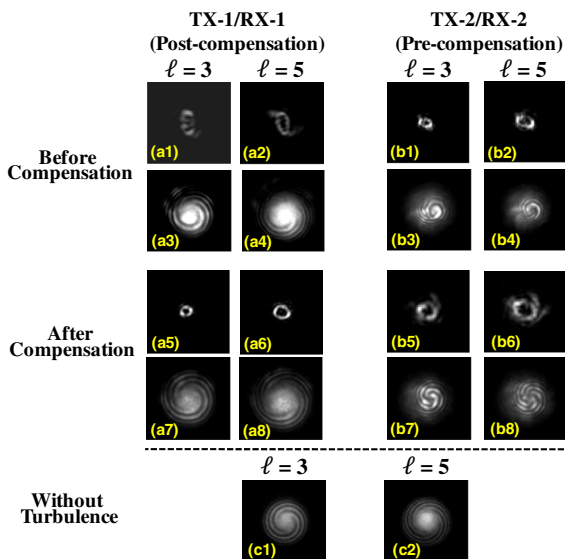

Fig. 5. (a) Received power of the OAM beam $\ell = 5$, under different turbulence realizations; (b) crosstalk from the OAM $\ell = 5$ channel to neighboring channels, under a random turbulence realization, with and without pre- or post-compensation.

resulting in severe crosstalk. Whereas with compensation, this crosstalk significantly decreases, and most of the incident power is better confined to the channel $\ell = 5$, as expected. Crosstalk values of the OAM channel $\ell = 5$, onto adjacent modes $\ell = 4$ and 6, decreases by about 14 and 14.5 dB for TX-1/RX-1, and 15.5 and 12 dB for the TX-2/RX-2 link, respectively. The crosstalk is calculated via dividing the received power of OAM channel $\ell = 4$ or 6 by that of channel $\ell = 5$.

To further quantify the performance improvement by using pre- or post-compensation, BER curves of OAM channel $\ell = 5$ (from branch ① or ③) for a fixed turbulence realization are measured for both links. Branches ② and ④ are turned on to introduce crosstalk effects from the neighboring channels. Since the amount of crosstalk is expected to depend on mode-spacing of the transmitted OAM modes Δ, the BER performance is investigated for $\Delta = 2$, 4. Branches ② and ④ are set to transmit a superposition of two equally weighted OAM beams, with either $\ell = 3$, 7 or $\ell = 1$, 9. Note that these two OAM beams in each branch carry the same data stream. Therefore, three OAM multiplexed channels, with either $\ell = 3$, 5, and 7 ($\Delta = 2$) or $\ell = 1$, 5, and 9 ($\Delta = 4$), are transmitted in each link direction. The recovered constellations of the 100 Gbit/s QPSK signal of channel $\ell = 5$, at optical signal-to-noise ratio (OSNR) of 23.5 dB for both links, with and without compensation, are shown in Figs. 6(a1)–(a8). Since smaller values of Δ result in higher crosstalk, it is expected that the constellations under $\Delta = 4$ [Figs. 6 (a3), (a4), (a7), (a8)] exhibit better quality than those of $\Delta = 2$ [Figs. 6 (a1), (a2), (a5), (a6)], for both the TX-1/RX-1 and TX-2/RX-2 links. We see that the constellations of each link become better after compensation, for both $\Delta = 2$ and 4.

Fig. 4. OAM beams $\ell = 3$, 5, before and after compensation of the TX-1/RX-1 link (post-compensation) and TX-2/RX-2 link (pre-compensation), respectively; (a1), (a2), (a5), (a6), (b1), (b2), (b5), and (b6) far-field intensity profiles; (a3), (a4), (a7), (a8), (b3), (b4), (b7), and (b8) interferograms; (c1) and (c2) interferograms of the OAM beams $\ell = 3$, 5 without turbulence.
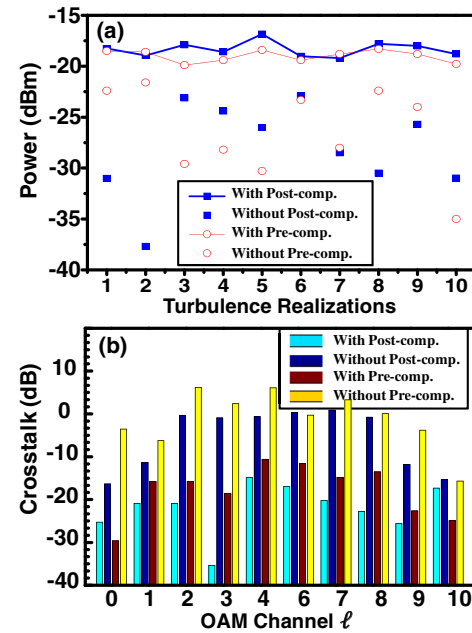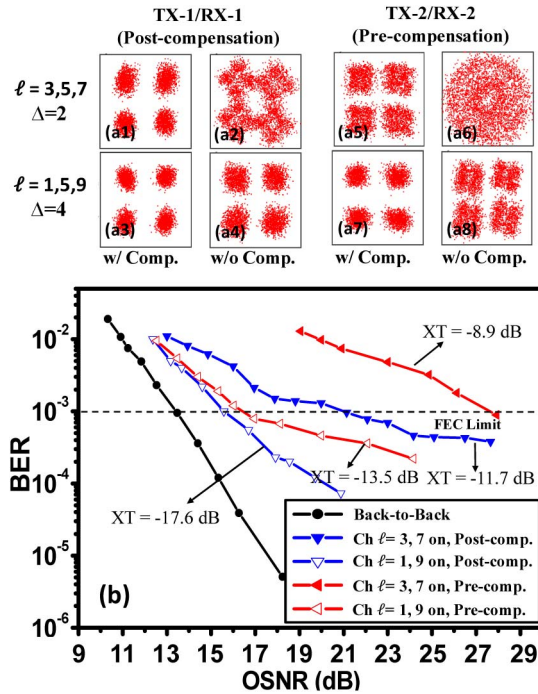
Fig. 6. (a1)–(a8) Recovered QPSK constellations of OAM channel $\ell = 5$, for TX-1/RX-1 and TX-2/RX-2 links; (b) BER for OAM channel $\ell = 5$, when transmitting three multiplexed channels ($\ell = 3, 5,$ and 7, with $\Delta = 2$, or $\ell = 1, 5,$ and 9, with $\Delta = 4$) under a random turbulence realization, with and without post-and pre-compensation; XT, crosstalk.

Figure 6(b) presents BER curves as a function of OSNR, for OAM channels $\ell = 5$, of TX-1/RX-1 and TX-2/RX-2 links, with and without compensation. With post-compensation, the measured crosstalk values for OAM channel $\ell = 5$, of the TX-1/RX-1 link under $\Delta = 2$ and 4, are improved from > -5 dB to -11.7 and -17.6 dB, respectively. For the pre-compensated TX-2/RX-2 link, the corresponding values are improved to -8.9 and -13.5 dB. The BERs without compensation are extremely high, due to severe crosstalk, and are not shown in Fig. 6(b). Here, an multiple-input–multiple-output equalization algorithm, that could help mitigate the channel crosstalk [31,32], is not used in the off-line DSP. However, we see that the BER curves for both links, after compensation, are all below the FEC limit of 1×10^{-3}, at OSNR values of 21 and 27.5 dB (for $\Delta = 2$), and 15.5 and 16.5 dB (for $\Delta = 4$), respectively. The TX-1/RX-1 link, with post-compensation, achieves better performance than the pre-compensated TX-2/RX-2 link by >1 dB, depending on the mode-spacing Δ.

5. DISCUSSION AND CONCLUSIONS

In this paper, we have demonstrated simultaneous pre- and post-compensation of multiple 100-Gbit/s data-carrying OAM beams, through emulated turbulence in a bidirectional link, by using a single adaptive optics compensation system. The experimental results show that the crosstalk between adjacent modes is reduced by >12 dB, at a random turbulence realization, and measured BERs reach below the FEC limit of 1×10^{-3}, after compensation for both directions of the link.

The post-compensated link achieves better BER performance than the pre-compensated link by >1 dB, as found from the experiment. However, according to our theoretical analysis, the two links (in principle) should have identical performance after compensation, if one is built symmetrically with the other one. The performance difference between the two links, observed from experimental results, may arise from the asymmetry or imperfection of the optics for OAM generation, or detection of the two links. Due to this asymmetry, the phase conjugation inside the AO system optimized for the post-compensated link may not be optimal for the pre-compensated link.

See Supplement 1 for supporting content.

REFERENCES

1. L. Allen, M. W. Beijersbergen, R. J. C. Spreeuw, and J. P. Woerdman, "Orbital angular momentum of light and the transformation of Laguerre-Gaussian laser modes," Phys. Rev. A **45**, 8185–8190 (1992).
2. A. Yao and M. J. Padgett, "Orbital angular momentum: origins, behavior and applications," Adv. Opt. Photon. **3**, 161–204 (2011).
3. J. Leach, E. Bolduc, D. J. Gauthier, and R. W. Boyd, "Secure information capacity of photons entangled in many dimensions," Phys. Rev. A **85**, 060304(R) (2012).
4. A. Mair, A. Vaziri, G. Weihs, and A. Zeilinger, "Entanglement of the orbital angular momentum states of photons," Nature **412**, 313–316 (2001).
5. G. Gibson, J. Courtial, M. Padgett, M. Vasnetsov, V. Pas'ko, S. Barnett, and S. Franke-Arnold, "Free-space information transfer using light beams carrying orbital angular momentum," Opt. Express **12**, 5448–5456 (2004).
6. J. Wang, J.-Y. Yang, I. M. Fazal, N. Ahmed, Y. Yan, H. Huang, Y. Ren, Y. Yue, S. Dolinar, M. Tur, and A. E. Willner, "Terabit free-space data transmission employing orbital angular momentum multiplexing," Nat. Photonics **6**, 488–496 (2012).
7. N. Bozinovic, Y. Yue, Y. Ren, M. Tur, P. Kristensen, H. Huang, A. E. Willner, and S. Ramachandran, "Terabit-scale orbital angular momentum mode division multiplexing in fibers," Science **340**, 1545–1548 (2013).
8. T. Su, R. P. Scott, S. S. Djordjevic, N. K. Fontaine, D. J. Geisler, X. Cai, and S. J. B. Yoo, "Demonstration of free space coherent optical communication using integrated silicon photonic orbital angular momentum devices," Opt. Express **20**, 9396–9402 (2012).
9. I. B. Djordjevic and M. Arabaci, "LDPC-coded orbital angular momentum (OAM) modulation for free-space optical communication," Opt. Express **18**, 24722–24728 (2010).
10. J. A. Anguita, M. A. Neifeld, and B. V. Vasic, "Turbulence-induced channel crosstalk in an orbital angular momentum-multiplexed free-space optical link," Appl. Opt. **47**, 2414–2429 (2008).
11. C. Paterson, "Atmospheric turbulence and orbital angular momentum of single photons for optical communication," Phys. Rev. Lett. **94**, 153901 (2005).

12. G. A. Tyler and R. W. Boyd, "Influence of atmospheric turbulence on the propagation of quantum states of light carrying orbital angular momentum," Opt. Lett. **34**, 142–144 (2009).

13. B. Rodenburg, M. P. J. Lavery, M. Malik, M. N. O'Sullivan, M. Mirhosseini, D. J. Robertson, M. Padgett, and R. W. Boyd, "Influence of atmospheric turbulence on states of light carrying orbital angular momentum," Opt. Lett. **37**, 3735–3737 (2012).

14. Y. Ren, H. Huang, G. Xie, N. Ahmed, Y. Yan, B. I. Erkmen, N. Chandrasekaran, M. P. J. Lavery, N. K. Steinhoff, M. Tur, S. Dolinar, M. Neifeld, M. J. Padgett, R. W. Boyd, J. H. Shapiro, and A. E. Willner, "Atmospheric turbulence effects on the performance of a free space optical link employing orbital angular momentum multiplexing," Opt. Lett. **38**, 4062–4065 (2013).

15. N. Chandrasekaran and J. H. Shapiro, "Photon information efficient communication through atmospheric turbulence—part I: channel model and propagation statistics," IEEE J. Lightwave Technol. **32**, 1075–1087 (2014).

16. Y. Ren, G. Xie, H. Huang, C. Bao, Y. Yan, N. Ahmed, M. P. J. Lavery, B. I. Erkmen, S. Dolinar, M. Tur, M. A. Neifeld, M. J. Padgett, R. W. Boyd, J. H. Shapiro, and A. E. Willner, "Adaptive optics compensation of multiple orbital angular momentum beams propagating through emulated atmospheric turbulence," Opt. Lett. **39**, 2845–2848 (2014).

17. B. Rodenburg, M. Mirhosseini, M. Malik, O. S. Magaña-Loaiza, M. Yanakas, L. Maher, N. Steinhoff, G. Tyler, and R. W. Boyd, "Simulating thick atmospheric turbulence in the lab with application to orbital angular momentum communication," New J. Phys. **16**, 033020 (2014).

18. K. Murphy, D. Burke, N. Devaney, and C. Dainty, "Experimental detection of optical vortices with a Shack-Hartmann wavefront sensor," Opt. Express **18**, 15448–15460 (2010).

19. C. Huang, H. Huang, H. Toyoda, T. Inoue, and H. Liu, "Correlation matching method for high-precision position detection of optical vortex using Shack–Hartmann wavefront sensor," Opt. Express **20**, 26099–26109 (2012).

20. J. H. Shapiro, "Reciprocity of the turbulent atmosphere," J. Opt. Soc. Am. **61**, 492–495 (1971).

21. D. L. Fried and H. T. Yura, "Telescope-performance reciprocity for propagation in a turbulent medium," J. Opt. Soc. Am. **62**, 600–602 (1972).

22. R. R. Parenti, J. M. Roth, J. H. Shapiro, F. G. Walther, and J. A. Greco, "Experimental observations of channel reciprocity in single-mode free-space optical links," Opt. Express **20**, 21635–21644 (2012).

23. J. H. Shapiro and A. L. Puryear, "Reciprocity-enhanced optical communication through atmospheric turbulence—part I: reciprocity proofs and far-field power transfer optimization," J. Opt. Commun. Netw. **4**, 947–954 (2012).

24. Y. Ren, H. Huang, G. Xie, C. Bao, L. Li, N. Ahmed, Y. Yan, M. Willner, M. P. J. Lavery, M. Tur, M. Neifeld, S. J. Dolinar, M. J. Padgett, R. W. Boyd, J. H. Shapiro, and A. E. Willner, "Simultaneous pre-and post-turbulence compensation of multiple orbital-angular-momentum 100-Gbit/s data channels in a bidirectional link using a single adaptive-optics system," in *OSA Frontiers in Optics* (Optical Society of America, 2013), paper FW6B.6.

25. R. Biérent, M. Velluet, N. Védrenne, and V. Michau, "Experimental demonstration of the full-wave iterative compensation in free space optical communications," Opt. Lett. **38**, 2367–2369 (2013).

26. J. D. Barchers and D. L. Fried, "Optimal control of laser beams for propagation through a turbulent medium," J. Opt. Soc. Am. A **19**, 1779–1793 (2002).

27. L. Andrews and R. Phillips, *Laser Beam Propagation through Random Media*, 2nd ed. (SPIE, 2005).

28. A. Ishimaru, *Wave Propagation and Scattering in Random Media*, 2nd ed. (Academic, 1978).

29. X. Zhu and J. Kahn, "Free space optical communication through atmospheric turbulence channels," IEEE Trans. Commun. **50**, 1293–1300 (2002).

30. J. Leach, M. R. Dennis, J. Courtial, and M. J. Padgett, "Vortex knots in light," New J. Phys. **7**, 1–11 (2005).

31. P. J. Winzer and G. J. Foschini, "MIMO capacities and outage probabilities in spatially multiplexed optical transport systems," Opt. Express **19**, 16680–16696 (2011).

32. R. Ryf, S. Randel, A. H. Gnauck, C. Bolle, A. Sierra, S. Mumtaz, M. Esmaeelpour, E. C. Burrows, R.-J. Essiambre, P. J. Winzer, D. W. Peckham, A. H. McCurdy, and R. Lingle, "Mode-division multiplexing over 96 km of few-mode fiber using coherent 6 × 6 MIMO processing," J. Lightwave Technol. **30**, 521–531 (2012).